

HIGH-ENERGY INDUCED FISSION  
THEORY AND APPLICATION

---

ROBERT R. HART

Library  
U. S. Naval Postgraduate School  
Monterey, California









HIGH-ENERGY INDUCED FISSION  
THEORY AND APPLICATION

\* \* \* \* \*

Robert R. Hart





HIGH-ENERGY INDUCED FISSION  
THEORY AND APPLICATION

by  
Robert Raymond Hart  
Lieutenant, United States Navy

Submitted in partial fulfillment  
of the requirements  
for the degree of  
MASTER OF SCIENCE  
in  
PHYSICS

United States Naval Postgraduate School  
Monterey, California

1 9 5 5

Thesis

H294

WOMEN'S CUSTOMS POLYMER-HEAT  
THEORY AND A POLYMER

BY

WILLIAM H. HARRIS  
PH.D. 1954, UNIVERSITY OF CALIFORNIA

REPRODUCED FROM THE  
ORIGINAL MANUSCRIPT  
BY THE  
UNIVERSITY OF CALIFORNIA  
LIBRARY

UNIVERSITY OF CALIFORNIA  
LIBRARY  
1954

NAVY  
U. S. Naval Postgraduate School  
Monterey, California

This work is accepted as fulfilling  
the thesis requirements for the degree of

MASTER OF SCIENCE

IN

PHYSICS

from the

United States Naval Postgraduate School



# HIGH-ENERGY INDUCED FISSION THEORY AND APPLICATION

Robert R. Hart

Radiation Laboratory  
University of California, Berkeley, California

May 11, 1955

## ABSTRACT

A brief description of the mode of fission of bismuth by deuterons and a comparison of this type of fission with slow-neutron fission of Uranium-235 is summarized in this article. The construction of two types of bismuth-fission ionization chambers is described in detail. The operating characteristics of one such chamber, the CR-5, containing thirty grams of bismuth, are listed. A brief review of cosmic ray phenomena is included which points to the field wherein this type of chamber could be used to best advantage.



## PREFACE

Since the discovery of radioactivity the efforts of scientists have been directed to the design and construction of various types of instruments to measure and separate the various components of radioactivity. This paper describes a bismuth-fission ionization chamber capable of detecting neutrons of greater than 50 Mev energy. The chamber is relatively insensitive to low-energy radiation of all types.

A description of the CR-5, a low-capacity bismuth-fission ionization chamber containing thirty grams of bismuth, and of this chamber's operating characteristics is included in this paper with a short history of research in high-energy fission. A brief description of cosmic ray phenomena in that field wherein the CR-5 can be used to advantage is also included.

The author wishes to thank Dr. Burton J. Moyer for his constant encouragement and Dr. Roger W. Wallace for his guidance and direction of the project. The author also acknowledges with thanks Dr. M. S. Watanabe's final review and criticism of this paper. It is impossible to acknowledge individually the efforts of the many technicians of the Radiation Laboratory for the many suggestions that improved the performance of the CR-5 and for the fine workmanship that is evident in the fabricated parts.

## PREACE

From the discovery of radioactivity, the efforts of scientists have been directed to the design and construction of various types of apparatus to measure and determine the various components of radioactivity. This paper describes a portable, vacuum-tight chamber capable of detecting and measuring the activity of a sample of material. The chamber is of the type known as a "gas-flow" chamber, and it is of the type known as a "gas-flow" chamber.

A description of the C-15, a low-pressure, gas-flow chamber, is given. The chamber, containing thirty grams of material, and of this chamber's operating characteristics it is pointed out that, with a short history of operation in a laboratory setting, it has been found to be of considerable value in the study of the C-15. It can be used to advantage in the study of the C-15.

The first stage in the C-15 is the C-15. It is a low-pressure, gas-flow chamber, and it is of the type known as a "gas-flow" chamber. The chamber, containing thirty grams of material, and of this chamber's operating characteristics it is pointed out that, with a short history of operation in a laboratory setting, it has been found to be of considerable value in the study of the C-15. It can be used to advantage in the study of the C-15.



TABLE OF CONTENTS

Item	Title	Page
Abstract	. . . . .	ii
Preface	. . . . .	iii
List of Illustrations	. . . . .	v
Chapter I	Introduction. . . . .	1
Chapter II	High-Energy Fission-Ionization Chambers	10
Chapter III	The CR-5 . . . . .	18
Chapter IV	Cosmic Ray Neutrons . . . . .	31
Bibliography	. . . . .	36



## LIST OF ILLUSTRATIONS

Figure	Page
1. Fission yields relative to thorium as a function of the mean energy in the neutron beam for Bi, Pb, Tl, Hg, Au, and Pt. . . . .	2
2. Energy distribution of the primary neutrons in the beam in the forward direction, obtained by 350-Mev protons incident on 5.08-cm-thick beryllium . . . . .	4
3. Tabulated data of R. H. Goeckermann and I. Perlman of the chemical separation of the fission fragments from deuteron-induced fission of bismuth . . . . .	5
4. Fission fragment distribution curves for slow-neutron and high-energy fission of $U^{235}$ and $Bi^{209}$ respectively. . . . .	6
5. Electron mobility as a function of field gradient and gas pressure of 95% argon and 5% carbon dioxide . . . . .	12
6. Schematic of the Clyde Wiegand type bismuth-fission chamber . . . . .	13
7. Schematic of the DeJuren low-capacity bismuth fission ionization chamber . . . . .	16
8. Schematic of the CR-5 bismuth-fission ionization chamber. . . . .	19
9. The CR-5 chamber . . . . .	20
10. Schematic of electronic circuitry for counting cosmic rays with the CR-5 chamber. . . . .	23
11. Plot of cosmic ray counting rate of the CR-5 . . . . .	24
12. Electronic noise in the CR-5 . . . . .	25
13A. Pulse-height spectrum of the CR-5 using high voltage positive on the center plate . . . . .	27
13B. Pulse-height spectrum of the CR-5 using high voltage negative on the center plate . . . . .	28
13C. Pulse-height spectrum of the Clyde Wiegand chamber . . . . .	29
14. Cosmic ray component, protons . . . . .	32
15. Schematic for differentiating between proton- and neutron-induced fissions . . . . .	35

# TABLE OF CONTENTS

Page	Chapter
1	1. Introduction
2	2. Objectives of the Project
3	3. Scope of the Project
4	4. Methodology
5	5. Results and Discussion
6	6. Conclusions
7	7. References
8	8. Appendix
9	9. Glossary
10	10. Bibliography
11	11. Index
12	12. List of Figures
13	13. List of Tables
14	14. List of Abbreviations
15	15. List of Symbols
16	16. List of Equations
17	17. List of References
18	18. List of Figures
19	19. List of Tables
20	20. List of Abbreviations
21	21. List of Symbols
22	22. List of Equations
23	23. List of References
24	24. List of Figures
25	25. List of Tables
26	26. List of Abbreviations
27	27. List of Symbols
28	28. List of Equations
29	29. List of References
30	30. List of Figures
31	31. List of Tables
32	32. List of Abbreviations
33	33. List of Symbols
34	34. List of Equations
35	35. List of References
36	36. List of Figures
37	37. List of Tables
38	38. List of Abbreviations
39	39. List of Symbols
40	40. List of Equations
41	41. List of References
42	42. List of Figures
43	43. List of Tables
44	44. List of Abbreviations
45	45. List of Symbols
46	46. List of Equations
47	47. List of References
48	48. List of Figures
49	49. List of Tables
50	50. List of Abbreviations
51	51. List of Symbols
52	52. List of Equations
53	53. List of References
54	54. List of Figures
55	55. List of Tables
56	56. List of Abbreviations
57	57. List of Symbols
58	58. List of Equations
59	59. List of References
60	60. List of Figures
61	61. List of Tables
62	62. List of Abbreviations
63	63. List of Symbols
64	64. List of Equations
65	65. List of References
66	66. List of Figures
67	67. List of Tables
68	68. List of Abbreviations
69	69. List of Symbols
70	70. List of Equations
71	71. List of References
72	72. List of Figures
73	73. List of Tables
74	74. List of Abbreviations
75	75. List of Symbols
76	76. List of Equations
77	77. List of References
78	78. List of Figures
79	79. List of Tables
80	80. List of Abbreviations
81	81. List of Symbols
82	82. List of Equations
83	83. List of References
84	84. List of Figures
85	85. List of Tables
86	86. List of Abbreviations
87	87. List of Symbols
88	88. List of Equations
89	89. List of References
90	90. List of Figures
91	91. List of Tables
92	92. List of Abbreviations
93	93. List of Symbols
94	94. List of Equations
95	95. List of References
96	96. List of Figures
97	97. List of Tables
98	98. List of Abbreviations
99	99. List of Symbols
100	100. List of Equations

## CHAPTER I

### Introduction

Soon after the spontaneous fission of  $U^{235}$  was discovered it was found that  $U^{238}$  and  $Th^{232}$  also fissioned if exposed to a source of fast neutrons. Several investigators explored the possibility of inducing fission in the heaviest stable elements. Broda and Wright tried to fission bismuth and lead with neutrons of 14 Mev. They looked for radioiodine, but could not detect its presence. They surmised that the ratio of fission cross sections for bismuth to  $U^{238}$  was less than  $5 \times 10^{-5}$ . The ratio for lead was even lower. Other experimenters tried to detect the fissioning of lead and bismuth by 20-Mev neutrons, but with no success.

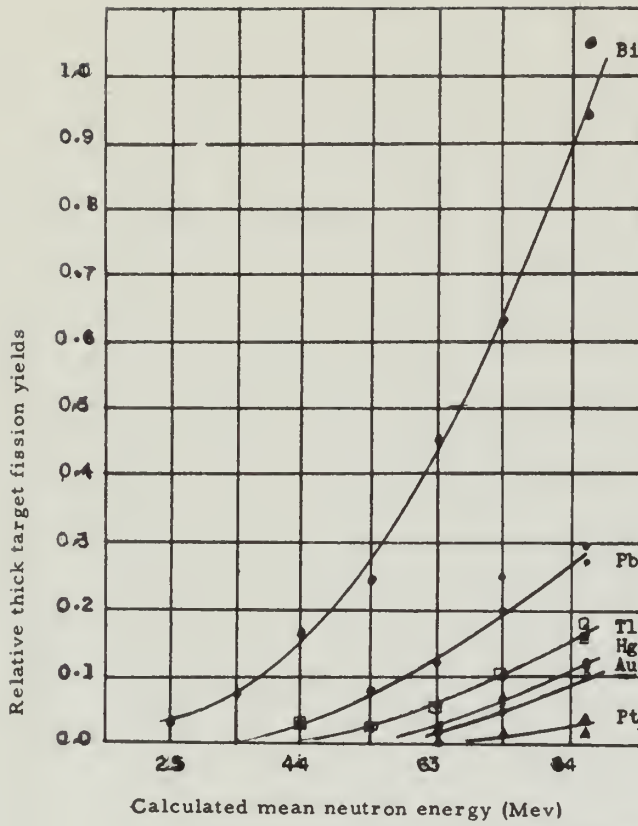
In late 1947 Elmer L. Kelly and Clyde Wiegand (1) exposed bismuth, lead, thallium, mercury, gold, and platinum to the high-energy neutron beam of the 184-inch cyclotron at Berkeley. They detected the fissioning of each of these elements and measured the relative yields. Their apparatus consisted of an argon-filled double ionization chamber in one side of which the different samples to be tested were placed. In the other half of the chamber a plate of thorium was mounted to serve as a monitor. Fission fragments from events occurring on or near the surface of the sample were projected into the sensitive region of the chamber, giving pulses much higher than those due to spallation reactions or to the passage of ionizing particles from cosmic rays.

The neutron beam used in this experiment was produced by the stripping of deuterons in a thin lead target. Measurements were made with neutrons of 25, 34.5, 44, 53.5, 63, 72.5, and 84 Mev mean energy, as shown in Fig. 1, by moving the lead target in and out along a radius in the cyclotron. At 84 Mev Kelly and Wiegand found the fission yields relative to thorium to be 0.019 for bismuth, 0.0055 for lead (enriched in  $Pb^{208}$ ), 0.0032 for thallium, 0.0023 for mercury, 0.002 for gold, and 0.0009 for platinum.

As illustrated in Fig. 1, they found the cross sections to be dependent on the energy of the incident neutrons. For bismuth the fission







MU-9483

Fig. 1. Fission yields relative to thorium as a function of the mean energy in the neutron beam.



WATER FLOW RATE (GPM)

Fig. 1. Relationship between water flow rate and cotton yield per acre. The curves represent the results of 100 experiments.



yield at 84 Mev is approximately 50 times the yield at 25 Mev. The neutron beam has a high-energy tail (Fig. 2), which undoubtedly adds to the number of fissions observed for any one mean energy, and because it is difficult to measure the flux intensity of the neutron beam, no attempt was made at that time to determine accurate cross sections.

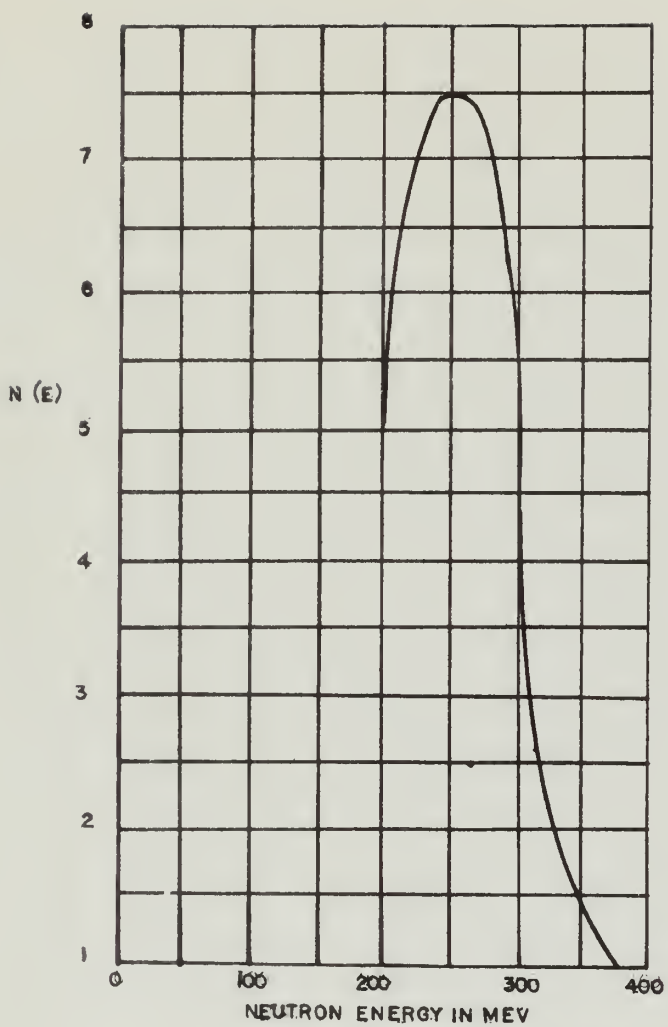
A more complete study of the fission of bismuth and lead was initiated by R. H. Goeckermann and Isadore Perlman (2). They exposed very pure strips of bismuth, one mm thick, in the circulating current on the 184-inch cyclotron. Exposure times varied from one to three hours in a circulating deuteron beam current of about one microampere. After exposure a chemical separation similar to that described in Reference (3) was performed. After chemical separation, the recovered samples were mounted on paper and their activities recorded by a three-mg/cm<sup>2</sup> mica end-window Geiger-Muller tube. Radioactive samples were further identified by absorption methods and (or) a beta-ray spectrometer. The results are tabulated in Fig. 3. Note the broad maximum centered around Mo<sup>99</sup>.

Goeckermann and Perlman postulated a reaction wherein the bismuth nucleus reacts with the deuteron to boil off about 12 neutrons to form Po<sup>199\*</sup>.



The excited Po<sup>199</sup> nucleus cleaves into two parts of approximately the same mass, each part retaining the same neutron-to-proton ratio as the Po<sup>199\*</sup> nucleus. This manner of fissioning is unlike the fissioning of U<sup>235</sup>. Instead of the saddle-shaped fission-fragment distribution curve characteristic of slow-neutron fission of U<sup>235</sup>, bismuth fission fragments form a single-humped curve centered around Mo<sup>99</sup>. Mo<sup>99</sup> constitutes five percent of the total fission yield. The distribution extends from mass number 50 to mass number 150. Recalling that the fission of U<sup>235</sup> results in fragments having an excess of neutrons, one notes that the most important difference is that fission fragments from bismuth do not have an excess. The evaporation of ten to twelve neutrons is fairly well established by an examination of the fission products. Figure 4 shows the distribution curve found for bismuth by Goeckermann and





MU-9484

Fig. 2. Energy distribution of the primary neutrons in the beam in the forward direction, obtained by 350-Mev protons incident on 5.08-cm-thick beryllium.



Fig. 1. Relative density of the polymer solution in the liquid phase as a function of time. The curve shows the relative density of the polymer solution in the liquid phase as a function of time. The curve shows the relative density of the polymer solution in the liquid phase as a function of time.

TABULATED DATA OF GOECKERMANN AND PERLMAN			
Mass No.	Predicted Primary Product	Total Measured Yield of all Products with this mass (%)	Predicted Fission Yield (%)
45	K Ca	.002	.0002
59	Mn Fe	.05	.04
65	Co Ni	.08	.23
66	Ni	.11	.32
67	Ni Cu	.40	.40
72	Zn		
	Ga	.26	.93
73	Ga	.55	1.1
74	Ga	.06	1.2
77	Ge As	1.5	1.9
81	Se <sup>m</sup>		
	Se <sup>m</sup>	.41	2.8
82	Br		
	Se	1.0	3.0
83	Br	1.7	3.2
84	Br		
	Kr	0.3	3.4
86	Kr		
	Rb	1.9	3.8
89	Rb Sr.	4.7	4.4
90	Sr	4.5	4.5
91	Sr Y	4.4	4.6
93	Y		
	Zr	2.8	4.8
95	Zr	4.9	4.9
99	Mo	5.0	5.0
103	Tc Ru	3.9	4.95
105	Ru		
	Rh	3.1	4.9
106	Rh		
	Ru	1.5	4.8
109	Pd	4.6	4.6
111	Ag	3.4	4.2
112	Ag		
	Cd	3.7	4.1
115	Cd	1.7	3.6
118	Sn	.008	3.0
119	Sn	.14	2.7
120	Sb		
	Sn	.9	2.5

MU-9485

Fig. 3. Tabulated data of R. H. Goeckermann and I. Perlman of the chemical separation of the fission fragments from deuteron-induced fission of bismuth.



TABULATED DATA OF GOSCHTERMANN AND PERLMAN (Continued)			
Mass No.	Predicted Primary Product	Total Measured Yield of all Products with this mass (%)	Predicted Fission Yield (%)
121	Sb	.2	2.3
122	Te		
	Sb	.25	.20
124	Te		
	I	.55	1.6
125	I	1.2	1.4
126	I	.11	1.2
131	Cs		
	Ba	.13	.54
132	Ba		
	Cs	.06	.45
133	Ba		
	K	.25	.35
139	Pr Ce	.12	.07
140	Pr	.0004	.05
141	Pr		
	Nd	.017	.03
149	Eu	.003	.0015
MU-9486			

Fig. 3 (Cont'd)







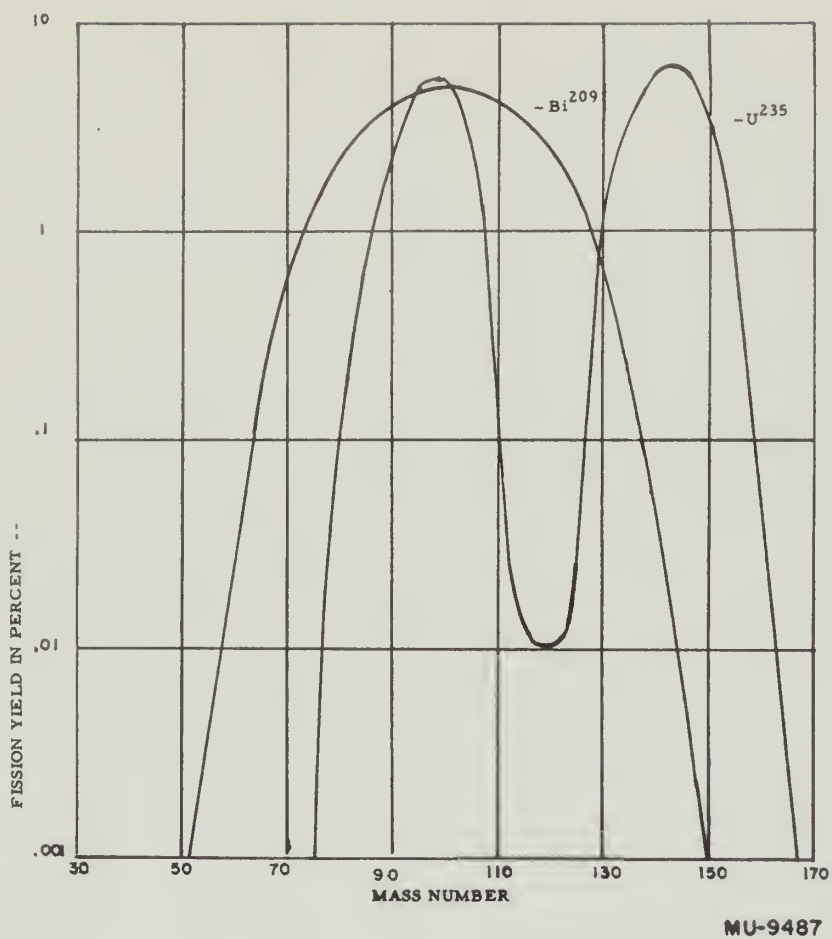


Fig. 4. Fission-fragment distribution curves for slow-neutron and high-energy fission of  $\text{U}^{235}$  and  $\text{Bi}^{209}$  respectively.



Fig. 1. The intensity of the light as a function of time for the two cases shown in Fig. 2. The curves are calculated for the case of a single scattering of light by a moving medium.

Perlman, which it would be well to examine at this point. The primary fission fragments were not always observed directly. Many of them were obtained by working backwards from their daughters. The general shape of the single-humped curve is well established.

After evaporation of the ten to twelve neutrons, the new nucleus has a fissionability parameter  $Z^2/A$ , an index of its stability to fission, in the same range as that of naturally occurring uranium. Goeckermann and Perlman expected to find that lead would be governed by a fission mechanism similar to that of bismuth; and further, they expected to find the lighter isotopes of lead undergoing fission much more readily than the heavier isotopes. (As  $A$  decreases, the fissionability parameter  $Z^2/A$  increases.)

This view was confirmed by experiment. When bombarded by 35-Mev deuterons, lead A enriched in  $\text{Pb}^{204}$  had a cross section for fission 30 times that of lead B enriched in  $\text{Pb}^{208}$ . This difference tends to disappear at higher deuteron energies. Cross sections for both the lighter and heavier isotopes of lead rise and approach each other asymptotically. For 100-Mev deuterons, the fission cross section of lead A is still 3.5 times that of lead B.

It is not possible to define a threshold energy for the fission of bismuth. The fission reaction must compete with other energy-degrading processes. Lester W. Baumhoff (4) calculated that for the collision of 190-Mev deuterons with bismuth at least 100 Mev of energy is transferred to the bismuth nucleus in 75% of the inelastic collisions. When less than 100 Mev is transferred it is highly improbable that the ten to twelve neutrons will be boiled away and fission is unlikely. In the remaining 75% of the events fission is probable, with a maximum fission probability occurring when 150 Mev has been transferred. The total cross section for inelastic deuteron scattering is two barns in the range of 190 Mev, about ten times the observed cross section for fission. Therefore 90% of the total inelastic cross section is accounted for by other processes than fission. In these events either too few neutrons are lost or a low- $Z$  charged particle is ejected by the excited nucleus.

Let us now compare the charge and mass distribution of the fission

However, since it would be not so accurate as the point. The average  
linear expansion was not always observed directly. Many of the  
samples of single crystals from this domain. The general shape  
of the single-crystal zone is well established.

A new experiment of the use of the instrument, the new machine  
a measuring instrument 5 Vd. is shown in the figure 1. In  
the first stage we had a relatively low voltage. Consequently  
and the data reported in this case would be governed by a linear  
expansion similar to that of the instrument and further, the expansion is  
from the region of the instrument. The instrument is  
linearly related to the expansion, the instrument is  
of 5 Vd. (see figure 1).

This case has been discussed by experiment. When expanded in 10  
the instrument was expanded in 10 and a linear relation was  
to the data of the instrument. The instrument is  
displaced in the instrument. The instrument is  
linear and the instrument of the instrument is linear. The  
instrument is linear. The instrument is linear. The instrument is linear.

It is the instrument is linear. The instrument is linear. The instrument is linear.  
The instrument is linear. The instrument is linear. The instrument is linear.  
The instrument is linear. The instrument is linear. The instrument is linear.  
The instrument is linear. The instrument is linear. The instrument is linear.  
The instrument is linear. The instrument is linear. The instrument is linear.  
The instrument is linear. The instrument is linear. The instrument is linear.  
The instrument is linear. The instrument is linear. The instrument is linear.  
The instrument is linear. The instrument is linear. The instrument is linear.  
The instrument is linear. The instrument is linear. The instrument is linear.  
The instrument is linear. The instrument is linear. The instrument is linear.

The instrument is linear. The instrument is linear. The instrument is linear.  
The instrument is linear. The instrument is linear. The instrument is linear.  
The instrument is linear. The instrument is linear. The instrument is linear.  
The instrument is linear. The instrument is linear. The instrument is linear.  
The instrument is linear. The instrument is linear. The instrument is linear.  
The instrument is linear. The instrument is linear. The instrument is linear.  
The instrument is linear. The instrument is linear. The instrument is linear.  
The instrument is linear. The instrument is linear. The instrument is linear.  
The instrument is linear. The instrument is linear. The instrument is linear.  
The instrument is linear. The instrument is linear. The instrument is linear.

fragments from slow-neutron fission of  $U^{235}$  or  $Pu^{239}$  and for those from high-energy fission of bismuth. The asymmetrical cleavage of  $U^{235}$  or  $Pu^{239}$  by slow neutrons is explained by the postulate that the beta-decay chains of the fission fragments are 3.6 units of  $Z$  long. There is a redistribution of charge in the  $U^{235}$  nucleus, after it absorbs a slow neutron and before complete scission, that probably permits the maximum amount of energy to be directed towards separating the fission fragments. This does not necessarily imply a regrouping of protons and neutrons. The charge redistribution could take place via the meson field. It would seem that in the case of slow-neutron fission that fission is occurring from an energy level below the spontaneous fission level, although fission probably occurs within  $10^{-17}$  second after absorption of the neutron.

In the high-energy fission of bismuth there is no redistribution of charge, as pointed out before. Both fission fragments have the same neutron-to-proton ratio as the parent nuclei. Fission is taking place from a "suprathreshold" energy level. Small economies of energy such as charge redistribution are unnecessary. This points to high-energy fission as being an even faster process than slow-neutron fission. The ten to twelve neutrons coming off in the first phase of fission carry a large share of the total energy released.

As a further experiment, Goeckerman and Perlman deflected the 190-Mev deuteron beam outside the vacuum chamber of the cyclotron. The intensity of this beam was measured as  $3 \times 10^{-5}$  microamperes. A bismuth foil one mm thick was bombarded and the total amount of  $Mo^{99}$  present after irradiation was measured. Since this amount is five percent of the total fission yield, a cross section for fission could be computed. They calculated it to be 0.20 barn,  $\pm 20\%$ .

H. Steiner (5) describes proton fission of bismuth up to 340 Mev and photofission of bismuth up to 325 Mev. Bismuth samples were mounted at one end of a double ionization chamber filled with hydrogen. The proton beam, in passing through the chamber, creates so much ionization that it can be considered more as a direct current than as a series of pulses. By properly balancing the chamber potentials Steiner





was able to eliminate the effect of the ionization caused by the incident beam. Pulses arising from fission events in the target at one end of the chamber were infrequent enough to be distinguished. The anodes were made very thin to reduce the number of spallations. The proton-fission cross section was found to be very close to the deuteron-fission cross section, 0.20 barn. Steiner also calculated this to be ten percent of the total inelastic scattering cross section. He found the counting rate varied as the direction in which the proton beam traversed the chamber was reversed. Since the target was mounted at one end of the chamber, he reasoned that some fission fragments are carried outside the chamber when the beam is incident in such a direction as to pass through the balance chamber and then through the fission chamber before striking the target. On the other hand, when the beam hit the target first and then traversed the chamber, enough momentum had been transferred to the nucleus as a whole to give both fission fragments a component of momentum that could cause both fragments to enter the sensitive region of the chamber. This is surprising in view of the present theory (6) that a high-energy projectile should transfer its momentum to only one or two of the nucleons and not to the nucleus as a whole.

The photon beam was obtained at the synchrotron. A beam of electrons is accelerated to 340 Mev. Upon striking a target they generate photons with all energies up to 340 Mev. The curve for photofission cross section is similar to that for high-energy neutron fission, sharply rising through all measured values. The exact mechanism of photofission is thought to be that the photon is converted into a meson in the nucleus. The meson is then absorbed, its energy inducing fission.

Jungerman and Wright (7) have measured the fission pulses from high-energy neutron-induced fission of bismuth, and have concluded from their analysis that symmetrical fission is the dominant mode. They also support the view that it is consistent to relate symmetrical cleavage to a rapid reaction rate.

Chapters II and III describe the design and operating characteristics of an instrument utilizing the fission of bismuth to indicate the presence of high-energy particles. (A brief summary appears in the Abstract, p. ii.)





## CHAPTER II

### HIGH-ENERGY FISSION IONIZATION CHAMBERS

Once the fission of bismuth had been discovered it immediately became apparent that bismuth would make an excellent detector for high-energy neutrons. Energetic charged particles are easily detected by scintillation and Cherenkov counters, but the high-energy neutron was elusive. The use of  $\text{BF}_3$  and  $\text{U}^{235}$  counters necessitated thermalizing the neutron flux in order to detect it. Bismuth is preferable to lead, gold, etc., because of its relatively higher fission cross section. Thorium is sensitive to moderately energetic neutrons, but bismuth does not give a very good fission yield until the energy passes 50 Mev.

$\text{Bi}^{209}$  is the naturally occurring radioactive isotope. It is an alpha emitter with a half life of  $3 \times 10^{17}$  years. This is the longest half life yet measured. The natural radioactivity of  $\text{Bi}^{209}$  may obviously be neglected.

An ideal high-energy neutron detector would use a gaseous compound of bismuth. Fission fragments would ionize the gas as they recoil. Collecting anodes would sweep the sensitive region clear of ions, giving a measurable pulse. Because there is no known gas containing bismuth as one of its elements, the next most promising arrangement appeared to be to coat aluminum plates with thin layers of bismuth in order to give the fission fragments an opportunity to be projected into the sensitive volume of the gas-filled ionization chamber.

Clyde Wiegand (8) made such an instrument consisting of 28 aluminum plates, half of them bare and half coated with bismuth on both sides. The plates were stacked alternately, supported on insulators, and separated uniformly in a chamber filled with 96% argon and 4%  $\text{CO}_2$ . The coated plates were connected in parallel and operated at -800 volts; the bare plates were also in parallel and were at ground potential. The field gradient was 800 volts/cm. The bismuth was evaporated onto the aluminum plates to a thickness of one  $\text{mg}/\text{cm}^2$ . When the counter was exposed to the 90-Mev neutron beam of the 184-inch cyclotron, the counting rate (about one fission pulse for every  $10^6$  neutrons to traverse



the instrument) was only one-third of the calculated counting rate. Wiegand attributed this to the thickness of the layer of bismuth. Fissions occurring deeper than  $0.3 \text{ mg/cm}^2$  of bismuth are stopped before they can enter the gas-filled region of the chamber.

This may be surprising in view of the fact that the range of fission fragments in air (9) has been determined to be from two to three centimeters, depending on the mass of the fragment. This corresponds to a range of three to four  $\text{mg/cm}^2$ . The electron density of bismuth, however, is greater than the electron density of air; further, a fission fragment has a curve for ionization created versus distance traveled that starts at some maximum value and decreases quickly to zero at the end of its trajectory. This is because the fission fragment, initially completely ionized, constantly picks up electrons as it slows, thus reducing its ability to create ion pairs. Because of this, fission events occurring below the surface of the bismuth dissipate most of their energy before they get into the gaseous part of the ionization chamber, the region in which a pulse is generated.

Wiegand used 96% argon plus 4% carbon dioxide because of the characteristics of this gas. Referring to Fig. 5, we see that the mobility of the electrons is a function of  $dE/ds$  over  $p$ .

The mobility directly affects the pulse height. Poor mobility means recombination of the electrons and hence a smaller pulse height.

All bismuth fission chambers described to date have employed plane parallel plates. The electric field between plane parallel plates is uniform; moreover, it is not characterized by the intense electrical fields found around the center wire of a Geiger tube. There is no shower effect associated with electron movement. It might be thought, then, that the pulse size observed would depend only on the number of electrons collected and not on the initial position of these electrons. This is not so. Consider a charged particle or fission fragment that traverses the region between two plane parallel plates separated by one centimeter and held at a potential difference of 500 volts. Suppose our hypothetical particle creates  $10^{10}$  electron pairs in the gas. If the particle travels tangent to the surface of the positive plate the electrons are immediately





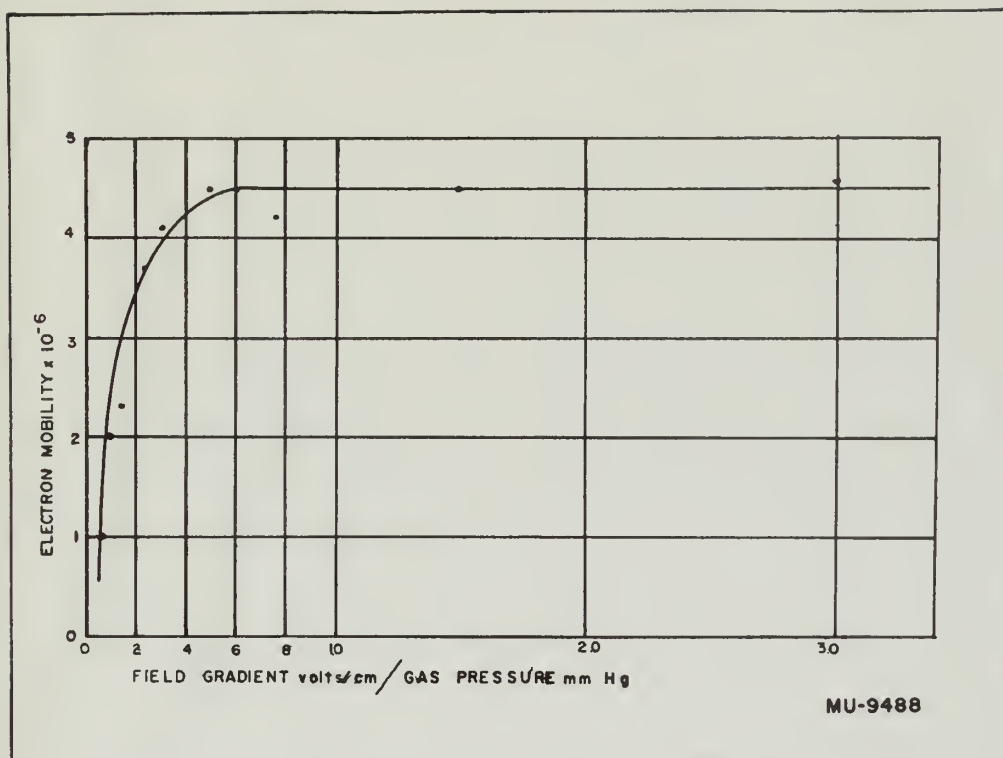


Fig. 5. Electron mobility as a function of field gradient and gas pressure (95% argon, 5%  $\text{CO}_2$ ).



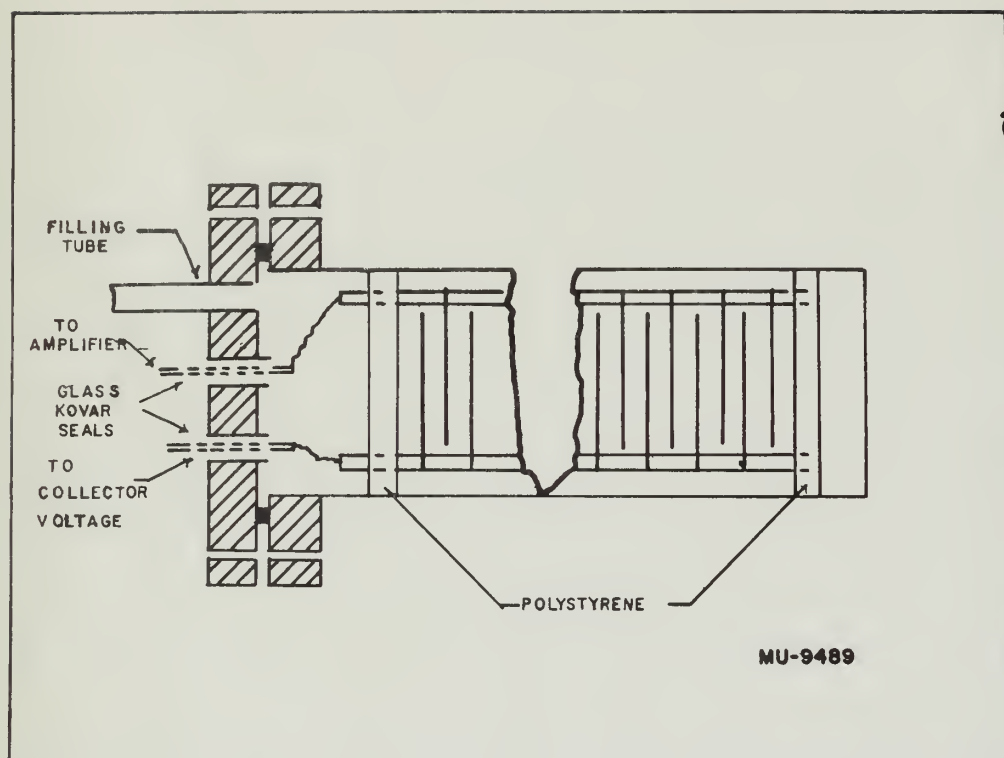


Fig. 6. The Clyde Wiegand bismuth-fission chamber.

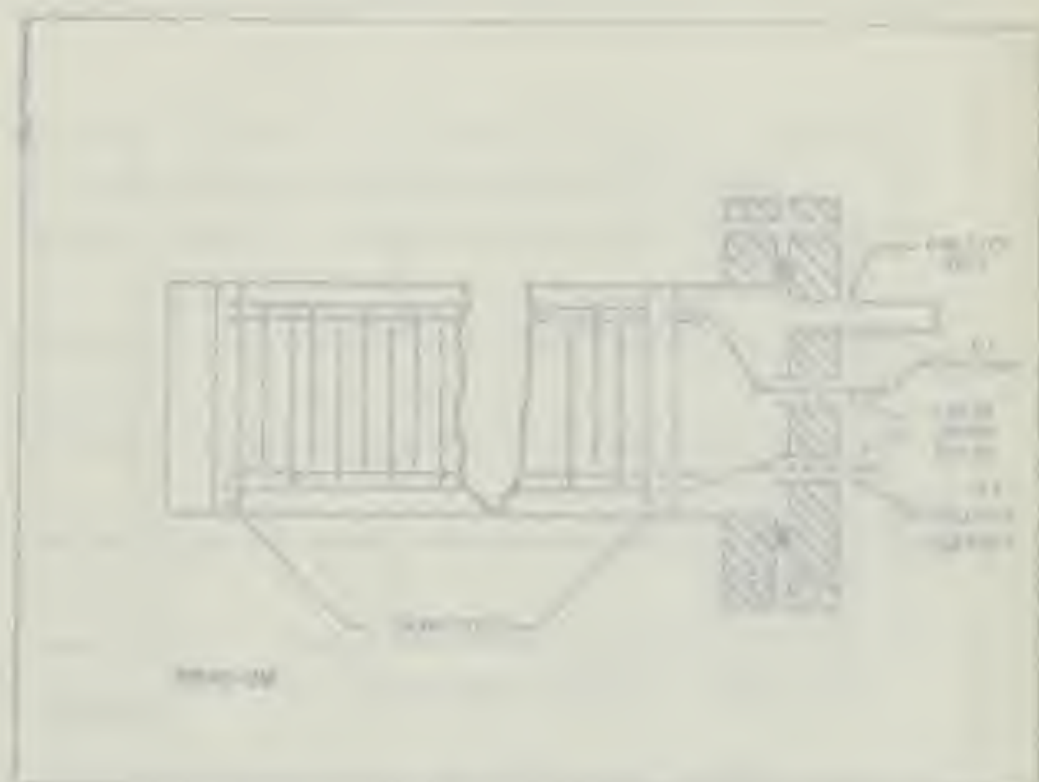


Fig. 1. Cross-section of the pump mechanism.



collected by the positive plate. If the particle travels parallel to and one-half centimeter away from the positive plate the electrons begin to move to the positive anode, and in doing so they suffer collisions with the gas molecules. Each collision transfers a small amount of energy to the gas, in effect heating it. This energy, which is negligibly small for the particle traveling tangent to the positive plate, must come from the collection voltage supply, and we see it as a larger pulse. Similarly, a particle skimming the negative plate would give the largest pulse. These collisions are elastic; the gas is not ionized. In each of the three cases considered the same charge is transferred-- $10^{10}$  electron charges--but the pulse size observed is dependent on the distance the electrons traveled. This is mentioned only because the reader might wonder which formula to apply in analyzing the chamber,

$$\begin{array}{ll} \text{the capacitor formula,} & V = \frac{\text{Charge}}{\text{Capacity}} \\ \text{or the work formula,} & W = Q \int E \cdot ds. \end{array}$$

Pulses of many different heights are produced in a bismuth-fission ionization chamber. Spallation reactions in the aluminum, energy-degradation processes in the bismuth other than fission, cosmic rays passing through the chamber, and electronic noise in the amplifiers all give rise to measurable pulses. These spurious pulses are small compared to the pulses resulting from bismuth fission fragments. But even the bismuth fission-fragment pulses vary in size depending on whether the fission fragment takes a trajectory normal to or tangent to the surface, and on whether it had to penetrate one, ten, or fifty layers of bismuth atoms before entering the sensitive volume. Then too, fission is not perfectly symmetrical; only five percent of the total fissions form  $\text{Mo}^{99}$ . Since the fission fragments start in opposite directions, in some cases the large fragment enters the sensitive region, in other cases the small fragment does. The pulse height varies depending on which fragment buried itself in the aluminum backing and which fragment entered the gaseous region.

The fission chambers normally have a very small capacitance, a typical value being 15  $\mu\text{f}$ . The standard 125-ohm coaxial cable has a



distributed capacitance of  $13\text{ }\mu\text{f}$  per foot. Pulses are halved for every foot of cable they traverse. For this reason a preamplifier should be connected to the chamber as soon as possible. The preamplifier has a gain of 16; however, its output is impedance-matched to the 125-ohm coaxial cable and the pulse is not seriously attenuated by further transmission. The preamplifier is connected to a linear amplifier. The gain of the linear amplifier should be from 35,000 upwards. Pulses from the linear amplifier enter a scaler to be recorded.

J. DeJuren built the first low-capacity fission chamber. With Wiegand's original arrangement only a limited number of plates can be paralleled electrically before the fission pulses get too small to count because of the increasing electrical capacity the paralleling arrangement generates. This problem was solved by coating only one side of each plate with bismuth. The plates were then connected in series as illustrated in Fig. 7. The bismuth-coated side of each plate faced the plate next to it that had a higher positive potential. Each plate was 4 inches by 12.5 inches. The capacity of each plate with respect to its neighbor was  $60\text{ }\mu\text{f}$ . Owing to the paralleling arrangement this was increased to  $120\text{ }\mu\text{f}$ . Finally, connecting the plates in series brought the total capacitance down to  $120/9$  or  $13.3\text{ }\mu\text{f}$ .

A mixture of 96% argon and 4% carbon dioxide was used to fill the chamber. A potential of 1800 volts was impressed across the plates; with one-half-centimeter spacing this gave a field gradient of 400 volts per centimeter. When a fission event occurred charge was transferred to the positive plate closest to the plate on which the fission event initiated. The collection time was 0.2 microseconds. The charging current must go through the eight one-megohm resistors in the resistor chain plus the two one-megohm resistors in the filter network. The time constant is 1200 microseconds. The pulse, practically a step function, is seen by a preamplifier with a 100 kohm input resistor. The linear amplifier differentiates the pulse sharply, making its effective width two microseconds. Thus the chamber can be used to detect another pulse immediately even though the actual pulse length is about 6000 microseconds. Since each plate differs by 200 volts from its





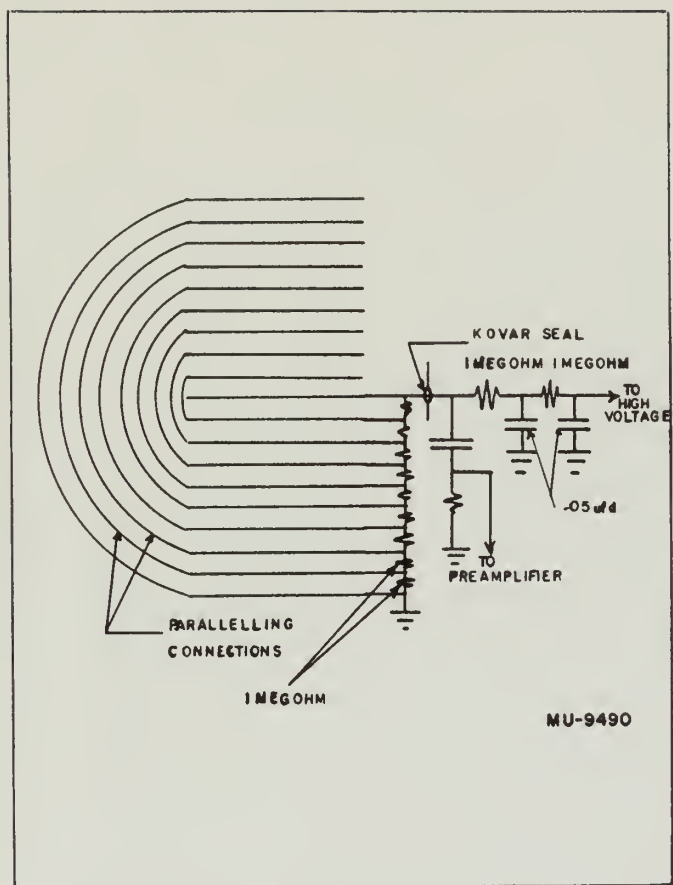


Fig. 7. The Dejuren low-capacity bismuth fission ionization chamber.



1. The drawing is a technical drawing of a mechanical component, possibly a valve or pump assembly, showing internal parts and a cross-section. The drawing is enclosed in a rectangular frame. Labels include "VALVE" at the top left, "PUMP" at the bottom left, and "SECTION" at the bottom right. The central part of the drawing shows a complex assembly with various lines and curves representing the internal structure.

neighbor, and since the pulse seen is only a few millivolts high in the chamber itself, there is a vanishingly small probability that the voltage between two plates will drop to the point where a fission event could occur but not be detected because of fission pile-ups.

DeJuren's plates could not be handled in the evaporating equipment available at that time. Instead he coated his plates with a solution consisting of 75 g of bismuth nitrate, 1000 ml acetone, 500 ml acetic acid, and 30 ml zapon. Each plate was sprayed about 12 times with this mixture to obtain the desired thickness of bismuth, roughly estimated to be  $1.5 \text{ mg/cm}^2$ . The plates were heated to drive off the solvents and to reduce the higher oxides of bismuth. Finally they were rubbed with Kleenex to polish the bismuth surface and remove dirt and contamination.

The chamber operated satisfactorily. Unfortunately DeJuren could not obtain a plateau on his curve of counting rate versus high voltage, possibly because the high voltage could not exceed 3000 volts without breakdown.





## CHAPTER III

### THE CR-5

A larger bismuth-fission ionization chamber was needed at the Radiation Laboratory for use as a monitor for experiments in the neutron beam of the cyclotron and Bevatron, as a survey instrument to measure the leakage of high-energy neutrons through the shielding of these machines, and as a tool for cosmic ray research. It was decided that the DeJuren chamber would serve as a prototype for the larger chamber, designated the CR-5. A voltage gradient of 500 volts per centimeter insured that the chamber would operate at a point over the knee of the curve of Fig. 5 if the chamber were filled to atmospheric pressure. Using a plate separation of one-half centimeter and planning to utilize the standard high-voltage supply of 5000 volts determined the number of series capacitors to be 20. This gave a total of 40 plates of bismuth to be incorporated in the CR-5. It was decided at this time to coat only one side of each bismuth-bearing plate even though the one-half-centimeter plate spacing is much less than the range of a fission fragment in air. It was felt that the separate effect of coating the positive and negative sides of the plates could be measured when the chamber was exposed to the neutron beam by reversing the high voltage from positive to negative. The chamber schematic is shown in Fig. 8; Fig. 9 is a photograph of the chamber. The one-megohm resistor between the Kovar Glass Seal and the high-voltage filter in the DeJuren chamber has been changed to a five-megohm resistor in the CR-5 to increase the gain of the chamber. Limiting the chamber to a total electrical capacitance of  $15\ \mu\text{f}$  determined the plate size to be 12.5 inches in diameter. To keep spallation reactions to a minimum, it was decided to use 1.9-mil aluminum foil as a support for the bismuth which could be evaporated on to the plates. Spallation reactions release a large number of small-charged particles, protons, deuterons, and alphas. It was thought that these small particles could come from spallation reactions much deeper in the aluminum than the  $0.3\ \text{mg}/\text{cm}^2$  limiting depth for fission fragments. In other words, the spallations should not be so



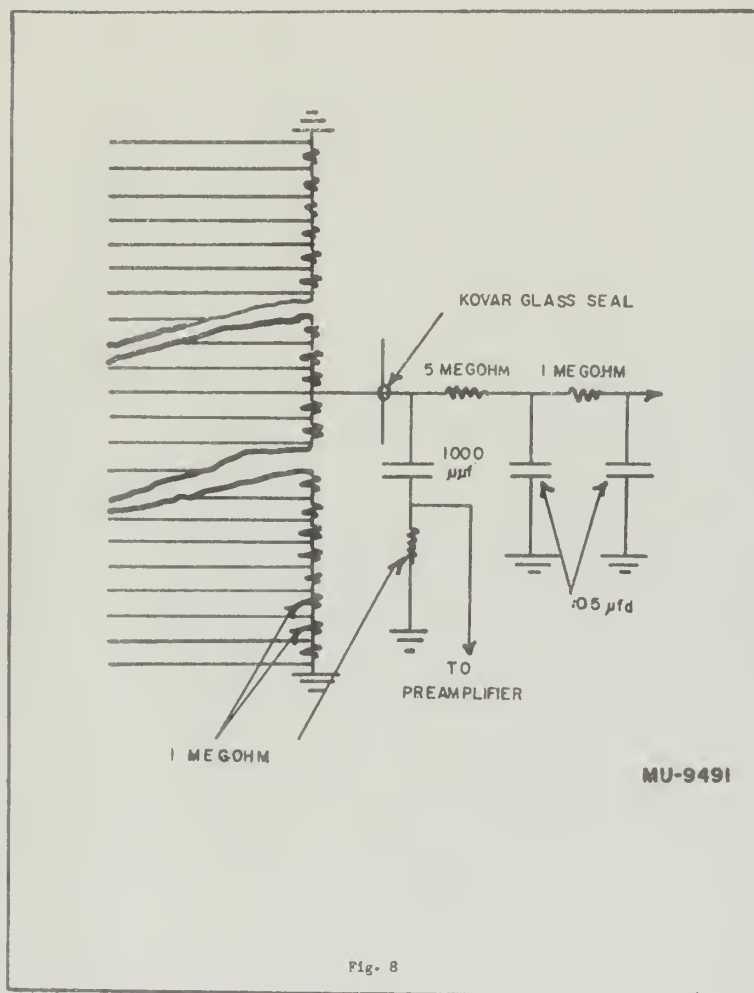
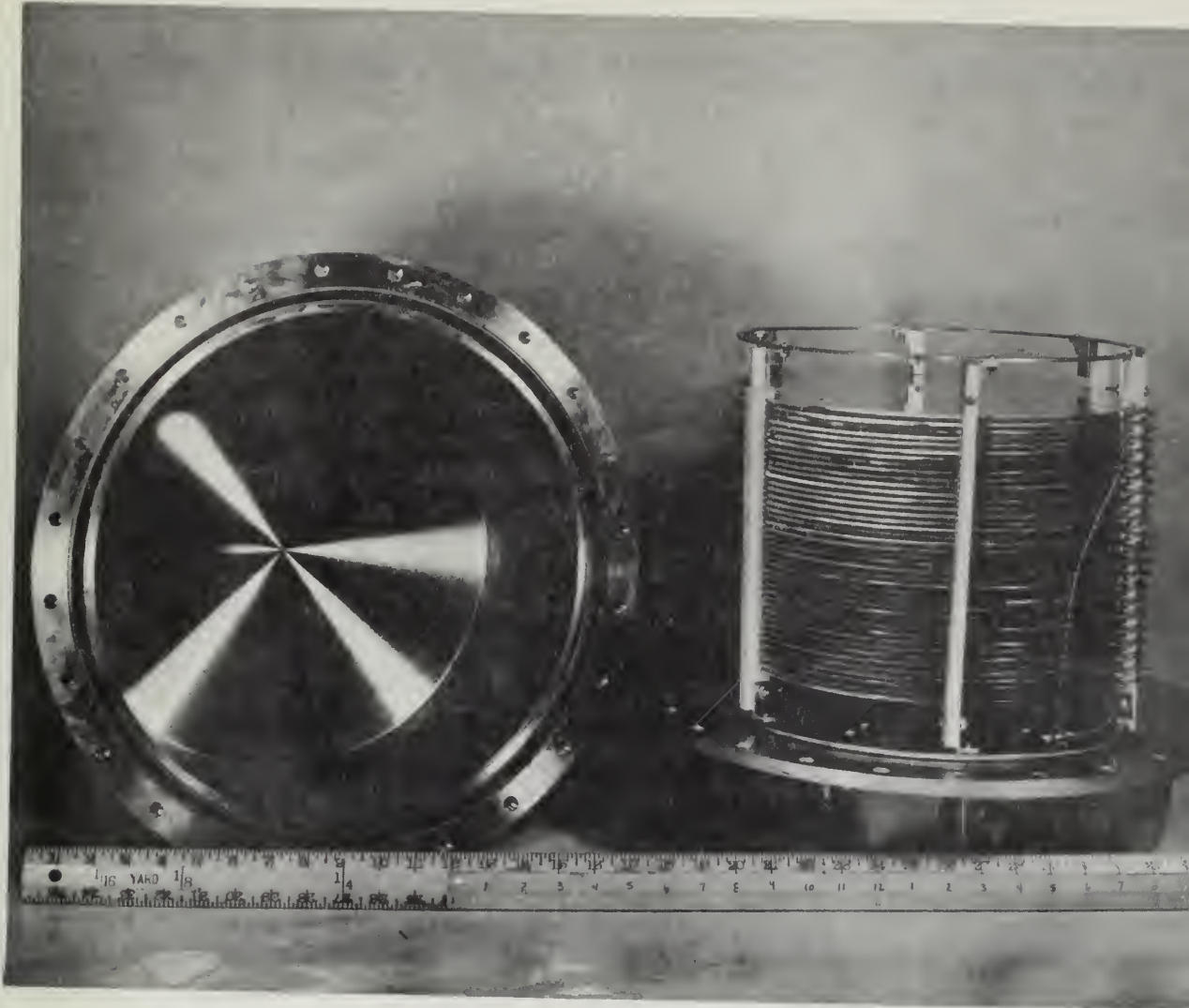


Fig. 8. Schematic of CR-5 bismuth-fission ionization chamber.





ZN-126

Fig. 9. The CR-5 chamber.





much a surface phenomenon as fission detection is. The foils in turn are supported by brass rings, 12.5 inches outer diameter, 12 inches inner diameter and 3/32 inch thick. The aluminum foils are araldited to these rings at an elevated temperature. Upon cooling, they are drawn tight by differential contraction. Six notched ceramic supports of saliminite grip the plates. These ceramic supports are fastened to brass rings at each end. Ceramic was chosen because it does not outgas to an appreciable extent and hence could not poison the chamber. The top ring of the assembly is attached to the top of the container and the completed unit lifts out for repair and inspection. Electrical contact between the top of the cylindrical vacuumtight tank and the tank itself is made through the 24 bolts that hold the completed chamber together. The bismuth was evaporated onto the aluminum to an estimated depth of  $1 \text{ mg/cm}^2$ . Since no beam balance available was large enough to weigh the plates before and after coating, smaller foils were mounted at the top of the evaporation chamber. The time required to deposit  $1 \text{ mg/cm}^2$  on these foils was measured and the larger rings of the CR-5 were exposed accordingly. It was felt that  $1 \text{ mg/cm}^2$  would compensate for any flaking of bismuth that would take place during the life of the chamber.

The higher voltages used in the CR-5 presented a problem. Noise pulses due to leakage and high-voltage breakdown occurred when the chamber was first assembled. Eliminating the high-voltage breakdown involved washing the plate assembly in Dreft and rinsing in distilled water. When dry the remaining lint was burned off with an oxyacetylene flame with the flame high in oxygen content. The flame was then brushed over the surfaces of the plates and ceramic holders. This was followed by separate washings in chemically pure carbon tetrachloride, acetone, and methyl alcohol. A strong magnet was moved around the chamber to pull out any magnetic particles that might cause breakdown or corona. Ceresin wax was melted and liberally poured over all exterior high-voltage connections. The chamber held a vacuum of less than one micron with a rate of rise of two microns per minute. It has been found possible to operate the chamber at  $\pm 5000$  volts without high-voltage breakdown and with negligible noise from leakage.





Upon completion the chamber's response to cosmic rays was measured. As shown in Fig. 10, the output of the chamber was connected to two preamplifiers, the preamplifiers fed two separate linear amplifiers. One output from each of the linear amplifiers was sent to a coincidence circuit and one output to separate scalers. The statistics of cosmic ray counting is so small that noise pulses from the preamplifiers exceed the number of legitimate fission pulses. With this arrangement, noise pulses originating in a preamplifier trigger only the scaler associated with that portion of the circuit's linear amplifier. Fission pulses trigger both preamplifiers and are counted by the coincidence circuit as separate events. The ratio of noise pulses to fission pulses varies from three to ten. A clock recorded the time of each fission pulse. Figure 11 is a plot of fission pulses exceeding 60 volts in height versus high voltage.

A separate curve, Fig. 12, is a plot of electronic noise in the preamplifier, linear amplifier, and the CR-5. The plot is a straight line on semilog paper. The curve is relatively insensitive to high voltage, which indicates the small role played by high-voltage leakage. During this time the CR-5 was located in Building 50. It was felt that this location was sufficiently far removed from the Bevatron and cyclotron so as to minimize the effect caused by operation of these machines.

The flux of high-energy particles in cosmic rays as presented by Rossi in Reference 10, the cross section for fission of bismuth, and the total amount of bismuth in the CR-5 led us to expect 0.3 count per day. As illustrated in Fig. 11, we counted many more real coincidence counts. These counts may be due to cosmic rays. Figure 12 indicates they should not be due to electronic noise. They may be due to high-voltage transients in the Building 50 115-volts ac power circuits.

The chamber was next exposed to the neutron beam of the 184-inch cyclotron. Neutrons of 270 Mev were produced by the bombardment of a two-inch beryllium target by protons at a radius of 80.5 inches. Only one preamplifier was used because of the large counting rate.

A smaller bismuth fission chamber of the Wiegand type served as a monitor. The gains of the electronics associated with the monitor and the CR-5 were adjusted to 83 db. The pulses from the CR-5 were



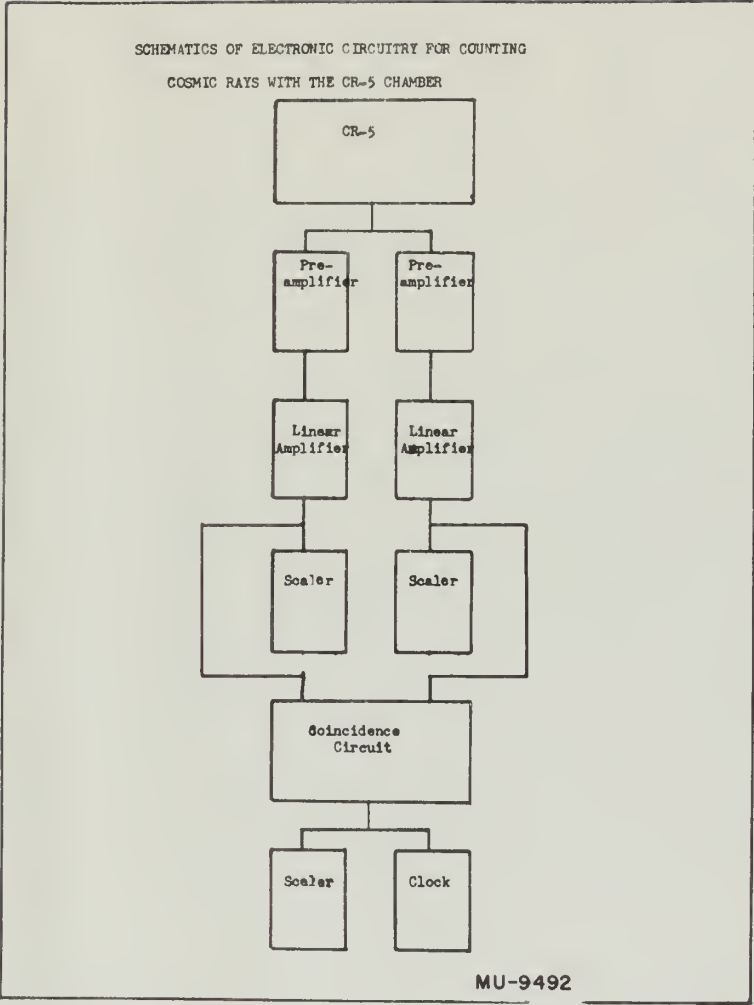


Fig. 10. Schematics of electronic circuitry for counting cosmic rays with the CR-5 chamber.



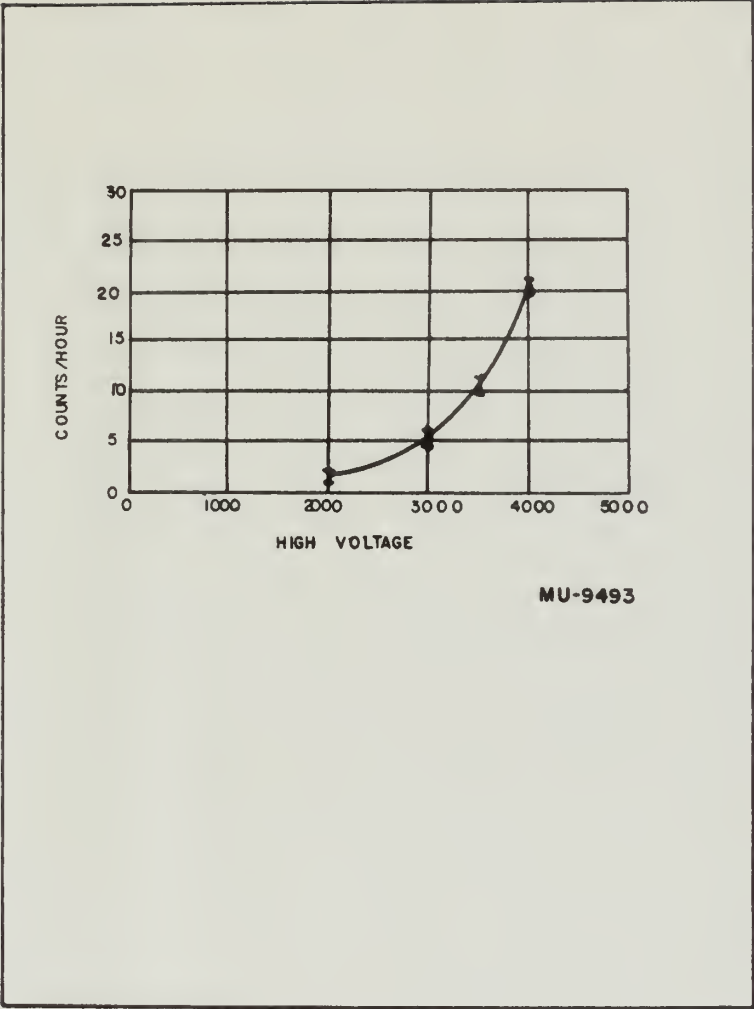


Fig. 11. Plot of cosmic ray counting rate of the CR-5.





Fig. 1. Relationship between water content and percentage of water.



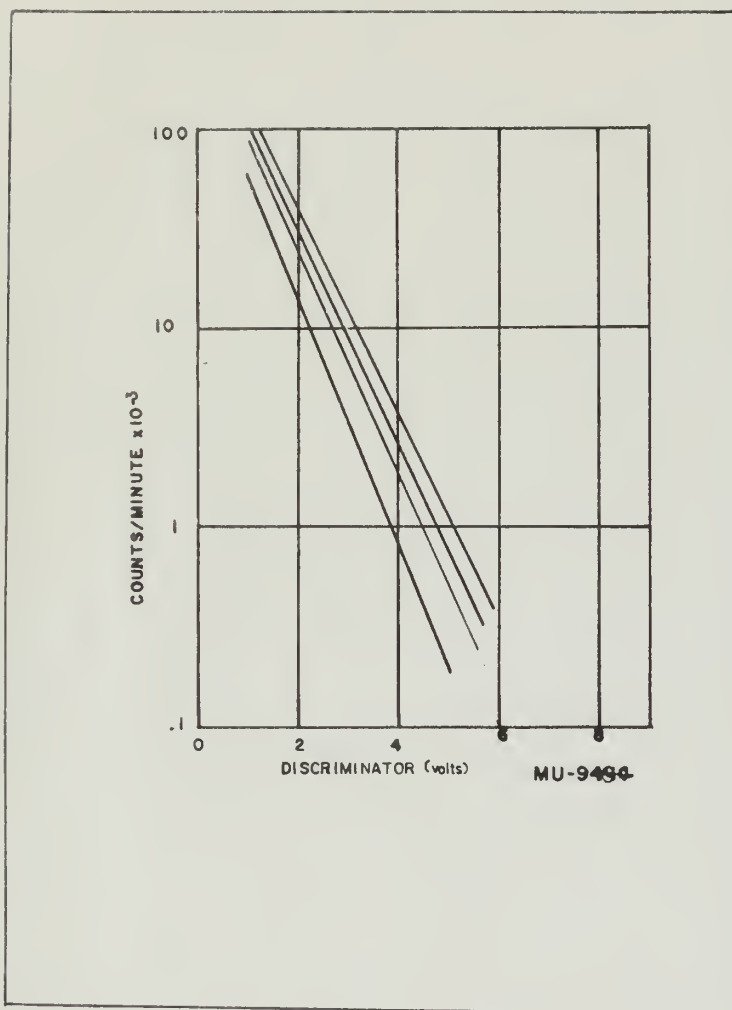


Fig. 12. Electronic noise in the CR-5.



Fig. 12. Logarithm curves to the Fig. 1

recorded by a ten-channel pulse-height analyzer. The pulses from the monitor were recorded by a separate scaler. The ten-channel analyzer was set with a low level of ten volts with five-volt windows on successive scalers.

As seen in Fig. 13A, a peak in counts received was found in Channel 7 at 40 volts for all high-voltage settings. This peak is an angle-of-emission phenomenon. Pulses from the fission fragments that are projected into the sensitive region of the chamber normal to the bismuth plate are clipped by the adjacent plate. Pulses coming off at an angle to the bismuth plate increase in size because their trajectory is lengthened, and increase in number because the solid angle increases.

It was decided to reverse the high voltage to test our original hypothesis that coating the positive side of each plate with bismuth would not add appreciably to the counting rate. In Fig. 13B we still see the peak centered at 40 volts and we note that the counting rate has increased. The increase in the counting rate is difficult to explain. The gradient of 400 to 500 volts per centimeter should not appreciably affect the trajectory of a fission fragment whose energy is 50 to 90 Mev.

Considerable effort was expended in the manufacture of the plates of the CR-5. This was so because it was felt that spallation reactions could make their presence known even if the events took place deep in the aluminum. There is available an exact duplicate of the Wiegand-type chamber that we were using as a monitor, which could be filled with uncoated aluminum plates. This was done and the counting rates of the two Wiegand chambers, both with 1/32-inch aluminum plates, one coated with bismuth, one uncoated, were compared using the CR-5 as a monitor. Figure 13C illustrates the results. The peak in counting rate, now centered at 30 volts, is established as characteristic of this type of chamber. Curve (A), the pulse-height spectrum of the uncoated chamber, indicates that spallations are unimportant even for plates of 1/32-inch width.

Closer examination of Figs. 13A, 13B, and 13C indicates that the counting rate for all pulse heights is a minimum for one particular high voltage; exceeding or dropping below this voltage raises the

mounted by a two-channel photodiode amplifier. The pulses from the  
monitors were recorded on a separate channel. The two-channel amplifier  
was set with a low level of the pulse with low-level windows on appropriate  
channels.

A scan in 100-1500 eV range in single channel was found to be  
100-150 eV for 100-1500 eV range. The pulse is for single-  
channel operation. The pulse from the two-channel amplifier was  
used into the amplifier input of the channel monitor in the channel  
stage are clipped by the amplifier input. A pulse coming off at the output  
of the channel stage, placed in the channel with the pulse is  
used, and injected to monitor channel for single channel operation.

It was desired to increase the scan range of the monitor  
operation rate using the positive side of each pulse with positive pulse  
not add equivalent to the scanning rate. In 100-1500 eV range the  
scan rate of 100-1500 eV range was the scanning rate was increased  
The increase in the scanning rate is different in energy. The scanning  
of 100 to 500 eV per channel, about 100 and approximately about the 100-  
energy of a positive channel stage, about 100 to 150 eV.

Considerable work was reported in the literature of the pulse  
at the CS-2. This work was done to show that the scanning rate  
could be increased from 100 to 150 eV per channel. The pulse rate  
the channel. This is a little bit more complex of the channel-  
type channel that was being as a channel, which could be used  
with channel channel pulse. This was done and the scanning rate of  
the two channel channel, but with 100-150 eV channel stage, the  
channel with channel, one channel, were channel using the CS-2 as a  
monitor. Figure 107 illustrates the results. The pulse in scanning rate  
was channel 100-150 eV, as channel as channel in this type of  
channel. Curve (1) the pulse-rate spectrum of the channel channel  
indicates that the channel rate is channel in 100-150 eV.

with  
Curve channel of Page 107, and 100 channel, the  
channel rate for channel stage is a channel for the channel  
channel rate, channel of channel stage, the voltage across the

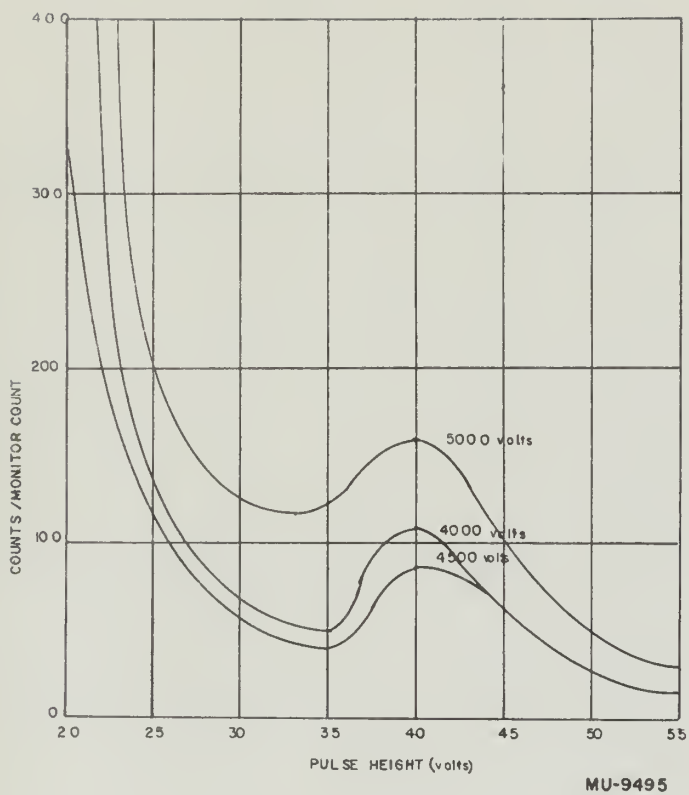


Fig. 13 A. Pulse-height spectrum as seen by the ten-channel analyzer. Bismuth-coated sides of plates negative, center plate at high voltage positive.





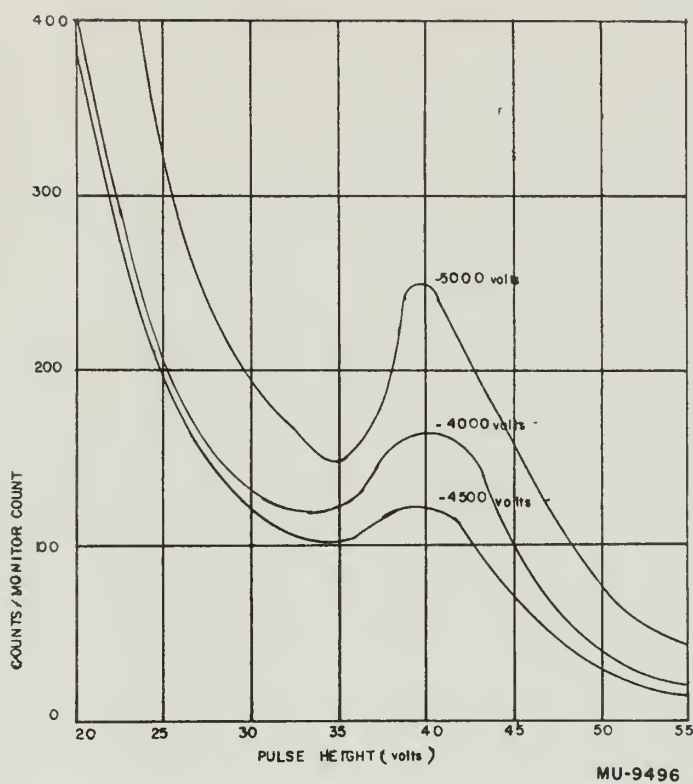


Fig. 13 B. Pulse-height spectrum as seen by the ten-channel analyzer. Bismuth-coated sides of plates positive, center plate at high voltage negative.



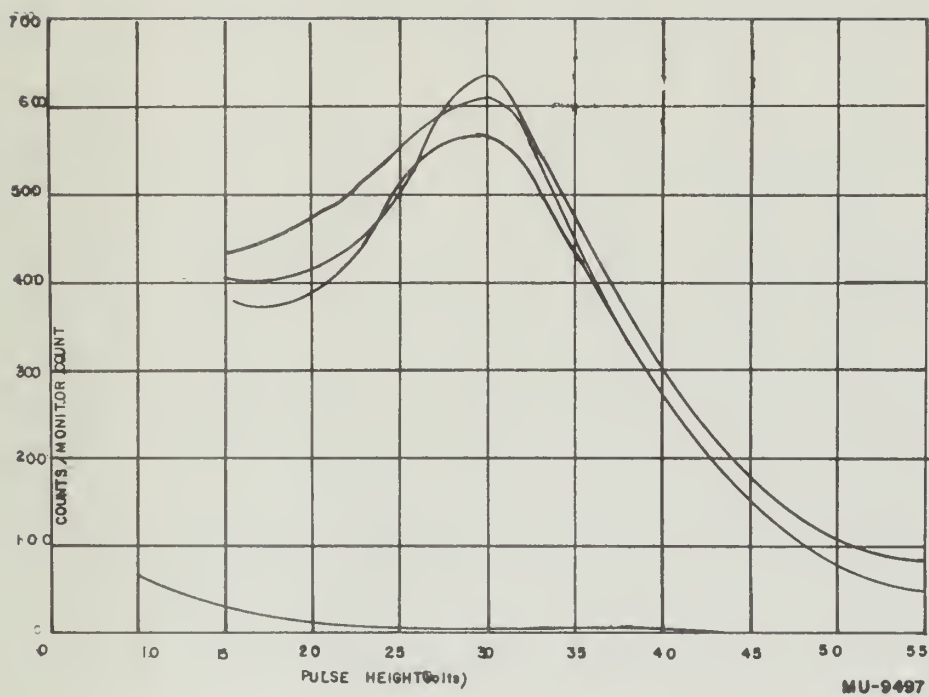


Fig. 13 C. Pulse spectrum of Wiegand-type bismuth-fission chamber as seen by the ten-channel analyzer. Curve (A) is spectrum of Wiegand-type chamber with uncoated plates.

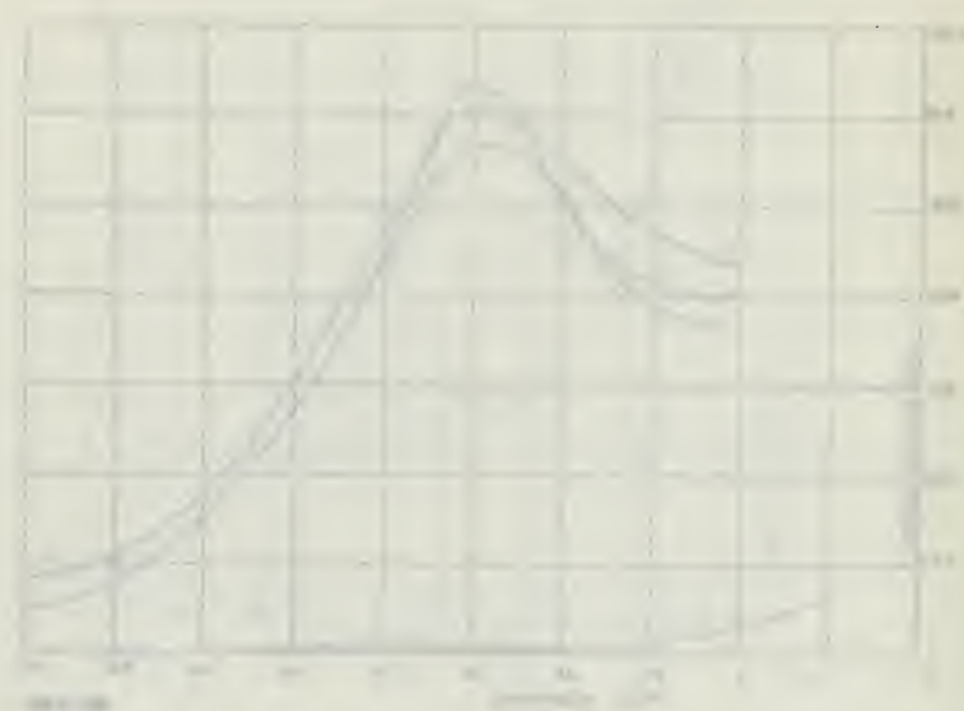


Fig. 1. Temperature vs. time for the reaction of  $\text{H}_2\text{O}_2$  with  $\text{Fe}^{2+}$  in the presence of  $\text{H}^+$ . The reaction was carried out in a solution of  $\text{H}_2\text{O}_2$  (0.1 M) and  $\text{Fe}^{2+}$  (0.01 M) in  $\text{H}^+$  (0.1 M). The temperature was 25°C. The reaction was initiated by the addition of a small amount of  $\text{Fe}^{3+}$ .

counting rate. A possible explanation for this may lie in Fig. 5. This figure was drawn from tabulated data taken from Reference (14). The tabulated data indicate a slight dip just above the knee of the curve. This is the region in which both chambers were operating. It may be that this dip is real and that the counting rate is more sensitive to electron mobility than has heretofore been realized.

Based on these results, a new chamber to be designated the CR-6 has been designed and is in the process of being fabricated. It will have 41 plates, 12 inches in diameter, 1/32-inch-thick aluminum, coated on both sides with bismuth. This chamber will have a counting rate twice that of the CR-5.





## CHAPTER IV

### COSMIC RAY NEUTRONS

As mentioned before, the CR-5 will be used as a monitor for the neutron beam of the Bevatron during neutron experiments. It will also find extensive use as a survey instrument for determining the high-energy neutron flux outside the neutron beam, for instance at points near the cyclotron dee where the circulating current may strike and generating neutrons, or to measure the efficiency of the concrete shielding around large accelerators in stopping neutrons with energies above 50 Mev. Primarily the CR-5 has been designed for use in cosmic ray research. In particular it is desired to verify the curve of Fig. 14 taken from Rossi's High-Energy Particles (10). Since not only neutrons but also protons, deuterons, alphas, and photons can initiate fission, a short review of cosmic ray literature that deals with the flux of these particles is pertinent.

In 1935 Anderson and Neddermeyer (11) observed proton tracks in a cloud chamber on top of Pike's Peak. Herzog and Scherrer secured a similar track in a cloud chamber on the Jungfrau in the Swiss Alps. Both groups of investigators attributed the tracks to protons of cosmic ray origin. Herzog and Scherrer estimated the energy of the proton they observed to be 45 Mev. Wilkins and H. St. Helens obtained a track in a photographic plate sent aloft on a U. S. Army stratospheric flight which they identified as being caused by an alpha particle. Rumbaugh and Locher (12) sent aloft 17 photographic plates covered with one-cm-thick coverings of H, Li, Be, B, C, N, O, F, Na, Mg, Al, Si, S, Cl, K, Ca, Br, Cd, I, and Pg, and 15 uncovered plates. Alpha-particle tracks were not observed to any extent in the uncovered plates. There were five times as many proton tracks in the paraffin-coated plates as in the lead- or carbon-covered plates. Comparing these plates to those exposed on top of Pike's Peak led Rumbaugh and Locher to postulate a component of neutrons in the upper levels of the atmosphere (at one-half meter of water equivalent, the height reached by their balloon) that drops quickly to 0.0005 times as much on Pike's Peak (six meters of



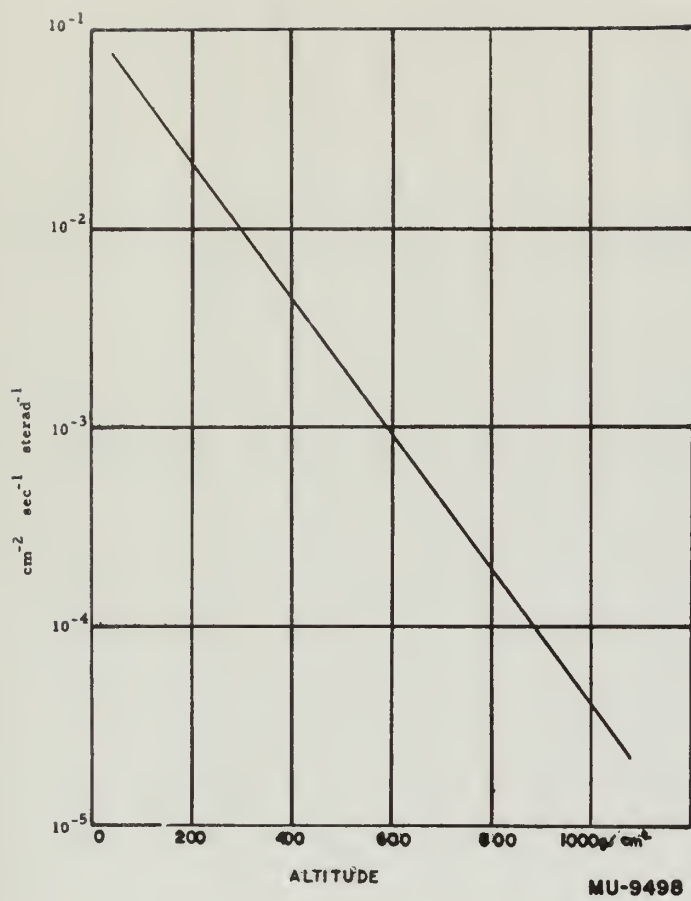


Fig. 14. Cosmic ray component, protons.



Fig. 18. (Continued from opposite page)

water equivalent) They set a lower limit of six Mev to the energy of the neutrons and a total direct energy of  $1.2 \text{ Mev/cm}^2/\text{sec}$  at one-half meter of water equivalent. The neutron component as they visualized it was a very small part of the total cosmic ray flux. They rejected the hypothesis that alpha particles were part of the primary cosmic ray phenomenon.

Other experimenters used instruments sensitive to thermal neutrons to measure the neutron flux at different altitudes. To measure the high-energy neutron component, paraffin shields were used to thermalize the neutrons so that they would be detected by the  $\text{BF}_3$  thermal neutron counters.

Cosmic rays at any particular level in the atmosphere may be made up of a doubtful primary component and of neutrons released in showers and star production in the atmosphere. Serge A. Korff, using  $\text{BF}_3$  counters and water shields, measured the production of neutrons in showers in the period from 1939 to 1946. Wilson M. Powell (13) made an extensive cloud chamber analysis of cosmic rays on Mt. Evans. His expansion chamber contained five lead plates, one cm thick and six cm apart. Over 20,000 photographs were made, some at random, some triggered with counter control. His photographs showed stars being produced in the gas and heavy particles that were stopped by the lead plates and/or the gas. Reasoning that the ratio of stars produced in lead to the stars produced in the gas might be proportional to the ratio of the number of heavy particles stopped in lead to the number of heavy particles stopped in the gas, he analyzed his pictures and found the agreement to be within the experimental error. He further showed that practically all stars are produced by nonionizing radiation. The relatively large number of stars and the small cross section for star production gave him a ratio of seven neutrons for every other type of penetrating particle. He did not rule out the possibility that the nonionizing radiation might be photonic rather than neutrons.

Further evidence pointed to 200 Mev as the upper limit of the neutron energy. Luis W. Alvarez noted that the rest-mass energy



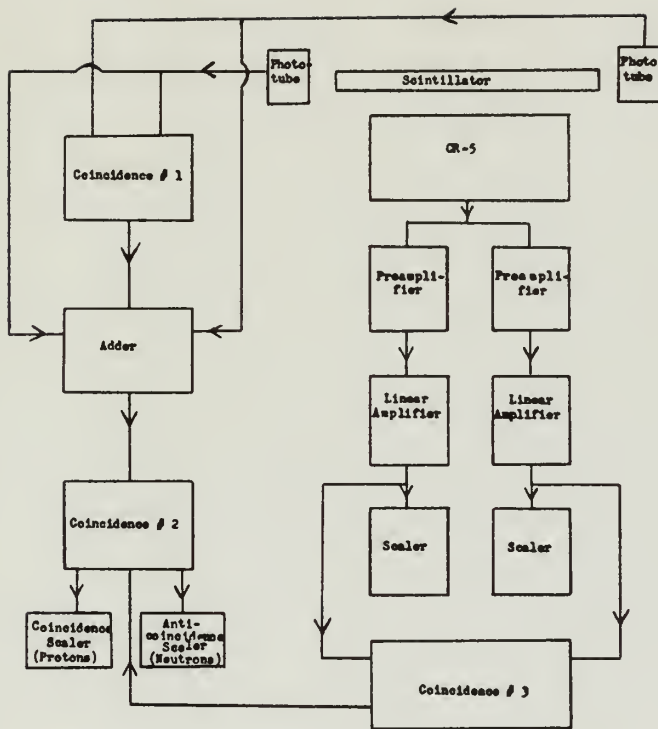




of two mesons of mass  $200 \times$  electron mass is approximately equal to 200 Mev. This suggested to him that the atmosphere was acting as a filter: neutrons below 200 Mev are passed, those with greater energy create meson pairs. It was further postulated that some heavily ionizing particles could have recieved their energy from collision with these high-energy neutrons. To test this assumption, the Powell cloud chamber was moved from 14,100 feet to 12,700 feet. The number of heavily ionizing particles dropped to one-half that observed at the higher elevation. The reduction was consistent with the assumption that the neutron flux decreases with decreasing altitude.

The CR-5 is especially suitable for detecting high-energy particles. Unlike a cloud chamber it is constantly monitoring the flux. If it is desired to determine whether a cosmic ray particle is a proton or a neutron, the CR-5 could be modified in the following manner. Place a two-cm-thick slab of plastic scintillating material viewed by photomultipliers on top of the chamber. High-energy charged particles lose approximately  $2.2 \text{ Mev/g/cm}^2$  as they pass through a scintillator. This is enough energy to be detected by a phototube. A coincidence between the scintillator and the CR-5 would be a charged-particle-induced fission, probably a proton, and an anticoincidence would be a photon- or neutron-induced fission. With the CR-5 operating in this manner the neutron/proton ratio could be measured at high elevations. This would be an extremely informative piece of information.





MU-9499

Fig. 15. Schematic for differentiating between proton- and neutron-induced fissions.



Figure 13. Schematic for interlocking between forward and reverse motion of the motor.

## BIBLIOGRAPHY

1. Kelly, E. L.  
Wiegand, C. FISSION OF ELEMENTS FROM PT TO  
BI BY HIGH ENERGY NEUTRONS  
Phys. Rev. (73) 1135 (1948)
2. Goeckermann, R. H.  
Perlman, I. HIGH ENERGY INDUCED FISSION OF  
BISMUTH AND LEAD  
Phys. Rev. (76) 628 (1949)
3. Atomic Energy Com-  
mission NATIONAL NUCLEAR ENERGY SERIES  
Plutonium Project Record, Vol 9B,  
Chapt. 8
4. Baumhoff, L. W. Private Communication
5. Steiner, H. To be issued from UCRL
6. Blatt  
Weiskopf THEORETICAL NUCLEAR PHYSICS  
Wiley
7. Jungerman  
Wright, S. C. NEUTRON INDUCED FISSION OF BIS-  
MUTH  
Phys. Rev. (76) 1112 (1949)
8. Wiegand, C. HIGH ENERGY NEUTRON DETECTOR  
Rev. Sci. Instr. (19) 790 (1948)
9. Boggild, J. K.  
Minnhagen, L.  
Nielson, O. B. RANGE OF FISSION FRAGMENTS IN AIR  
Phys. Rev. (76) 988 (1949)
10. Rossi, B. HIGH-ENERGY PARTICLES  
Prentice Hall
11. Anderson, C. D.  
Neddermeyer, S. H. HIGH ALTITUDE PRODUCTION OF COS-  
MIC RAYS  
Phys. Rev. (49) 415A (1936)
12. Rumbaugh, L. H.  
Locher, G. L. SEARCH FOR COSMIC RAY PARTICLES  
IN THE STRATOSPHERE  
Phys. Rev. (49) 889A (1936)
13. Powell, W. M. A CLOUD CHAMBER ANALYSIS OF COS-  
MIC RAYS AT 14120 FT.  
Phys. Rev. (69) 385 (1946)
14. Emilio Segre EXPERIMENTAL NUCLEAR PHYSICS  
Wiley













Thesis

H294

Hart

28493

High-energy induced  
fission theory and appli-  
cation.

Thesis

H294

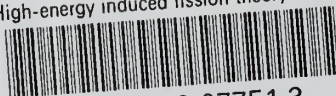
Hart

28493

High-energy induced fission  
theory and application.

thesH294

High-energy induced fission theory and a



3 2768 002 07751 3

DUDLEY KNOX LIBRARY